J Mater Sci (2007) 42:9359–9365
DOI 10.1007/s10853-007-1856-7

Synthesis of bulk metallic glass composites using high oxygen containing Zr sponge

Ranadeep Bhowmick · Bhaskar Majumdar · Dinesh K. Misra · Upadrasta Ramamurty · K. Chattopadhyay

Received: 27 February 2007 / Accepted: 15 May 2007 / Published online: 27 July 2007

Abstract The effect of large concentration of oxygen on the microstructural development of Zr–Cu–Al–Ni bulk metallic glass (BMG) alloys, prepared from commercially available Zr sponge, has been studied. Apart from promoting crystallization, increased concentration of oxygen (~8000 ppm) spawns additional phases. In particular, we report the appearance of α-Zr, dendritic Zr_2Cu phase and the Zr_2Ni type cubic phases. Addition of oxygen scavenger like Yttrium only partially solves the problem. Phase evolution was also found to be sensitive to the cooling rate and hence to the thickness of the cast sample. Thus it is possible to produce a gradient microstructure with predominantly amorphous phase at the outer layer.

Introduction

Due to their unique combination of mechanical properties, bulk metallic glasses (BMGs) have been receiving considerable research interest recently. Almost all of the BMG alloy systems that are currently being pursued from an application perspective, particularly those based on transition group metals, are cast from high purity elements. This is necessary to keep the oxygen content low as the transition metals are good oxide formers. Several investigators have explored the role of oxygen on the glass forming ability (GFA) and crystallization behavior of Zr-based glasses [1–9]. Oxide phases induce crystallization at higher temperatures and shorter incubation times [1]. Eckert et al. [2, 3] established that for bulk specimens, oxygen triggers the formation of nanocrystalline FCC $NiZr_2$-type phase. These nanocrystals act as heterogeneous nucleation sites for the crystallization of other stable intermetallic phases. Murty et al. [4] reported a two step crystallization process for melt spun ribbons with higher oxygen content as compared to a polymorphous crystallization of amorphous phase to Zr_2(Cu, Al) at lower oxygen concentrations. Liu et al. [6] has shown that oxygen level of 3000 ppm completely deteriorates the mechanical performance of the BMG and the microstructure contains predominantly crystalline phases. In contrast, there are reports of formation of metallic glass in high oxygen containing alloy processed by melt spinning [10]. Besides oxygen concentration, the cooling rate also influences the microstructural evolution [2, 11, 12]. Formation of metallic glass in high oxygen containing alloy by melt spinning and the absence of crystalline phases in wedge shaped specimens with smaller angle, are evidences of the effect of cooling rates. Zhang et al. [5] and Liu et al. [6] have demonstrated the beneficial effects of microalloying in reducing the adverse effects of oxygen on the GFA of the Zr-based glasses. The microalloying elements were chosen since they are known for their strong tendency to form oxygen-rich glass phases. Recently a detailed investigation established that the ductility of BMG disappear for an oxygen content as low as 600 ppm [6].

Most of the investigations to date in this area focused on the effect of small amount of oxygen on the formation of Zr based BMG. The microstructural evolution in the presence of larger oxygen content is not well studied. Also since

R. Bhowmick · D. K. Misra · U. Ramamurty · K. Chattopadhyay (✉)
Department of Materials Engineering, Indian Institute of Science, Bangalore 560012, India
e-mail: kamanio@materials.iisc.ernet.in

B. Majumdar
Defense Metallurgical Research Laboratory, Kanchanbagh, Hyderabad 500058, India

high purity elements are expensive, the BMGs formed also tend to have cost disadvantage, offsetting the performance advantage. Therefore it is instructive to examine the possibility of forming Zr-based BMGs and particularly BMG composites with commercial purity Zr. Since oxygen content of commercial Zr sponge is high and often contains oxides at the surface, it is relatively easy to incorporate large amount of oxygen in the melt. In this paper, we explore the possibility of making α-Zr-based BMGs with the commercial purity Zr sponge containing high (~8000 ppm) oxygen content and focus on the microstructure development including the effect of section thickness and hence cooling rate. We have chosen for the present work Zr–Cu–Al–Ni alloys, which have been studied extensively because of their large super cooled region and high GFA [13, 14].

Processing and characterization

Three alloy compositions, namely $Zr_{55}Cu_{30}Al_{10}Ni_5$, $Zr_{60}Cu_{20}Al_{10}Ni_{10}$ and $Zr_{65}Cu_{15}Al_{10}Ni_{10}$, have been synthesized during present investigation. These compositions are well known glass formers, so the ease or lack of GFA will solely depend upon the oxygen present in them. In addition, we have also prepared an alloy $Zr_{53}Cu_{19}Ni_{10}Al_{10}Ti_5Y_3$ containing small amount of Y and Ti in an effort to getter the oxygen from the melt. Commercial purity Cu and Ni, 99.9% purity Al, and commercial Zr sponge were used. The alloys with composition $Zr_{53}Cu_{19}Ni_{10}Al_{10}Ti_5Y_3$ have also been prepared with pure zirconium for comparison. Pellets of Zr were produced by vacuum arc melting under an inert Ar atmosphere. To prepare the BMG samples, the master alloy was remelted by induction heating and then pressure cast into Cu mould. Three types of moulds, namely wedge shaped, cylindrical and plate were used for the BMG casting, to assess the role of cooling rate. The wedge shaped mould is rectangular (8×7 mm^2) at the top face tapering to a point at the bottom; the height of the mould is 50 mm. The diameters of the cylindrical moulds used are 3 and 5 mm, both with a height of 30 mm. Two types of plate shaped moulds were used, with casting dimensions $1 \times 5 \times 25$ mm^3 and $2 \times 5 \times 25$ mm^3. In case of $Zr_{53}Cu_{19}Ni_{10}Al_{10}Ti_5Y_3$ alloy cylindrical rods of diameter 4 mm and length of around 70 mm were processed from the pre-alloyed melt by suction casting into a copper mould.

The as-cast samples were characterized to evaluate the extent of glass formation in each of them. Differential Scanning Calorimetry (DSC) (METTLER TOLEDO 822^e) was used to determine whether the as cast samples contains a glassy phase, identified by a glass transition. Electron Probe microanalysis (Cameca make, SX 100 series) was conducted to determine quantitatively the amount of oxygen present in the as cast alloys. X-Ray diffraction (XRD) patterns of the as cast samples were obtained using Cu-Kα radiation from the specimens cut parallel to the broad face of the samples using a JEOL JDX-8030 X-ray diffractometer system. Microstructural information was obtained using optical microscopy, scanning electron microscope (JEOL JSM-840A, Sirion FEI) and transmission electron microscope (Tecnai-F30). The gradient of mechanical properties was evaluated by using an instrumented microindenter (Zwick Roller system).

Results

Characterization of the castings

The microprobe analysis estimates the oxygen content of the alloys prepared with commercial Zr sponge ranges between 8,000 and 9,000 ppm (i.e., 0.8–0.9 at.%). Figure 1a shows the optical micrographs of the as-cast wedge shaped sample of $Zr_{55}Cu_{30}Al_{10}Ni_5$ alloy taken from three different regions (as shown in the schematic). The tip portion of the wedge shaped sample is almost glassy but an increase in volume fraction of crystalline phases with increasing casting dimensions can be observed, indicating a cooling rate sensitive microstructure. Figure 1b shows the XRD pattern obtained from an area close to the tip of the wedge shaped sample. The XRD traces confirm that it is predominantly amorphous. Figure 1c shows a DSC scan of the tip portion of the sample at a heating rate of 10 K/s. A distinct glass transition can be seen. The difference between glass transition temperature, T_g (408 °C) and crystallization temperature, T_c (488 °C) is 80 °C, with a single crystallization exotherm. The onset temperature is similar to that reported by Conner et al. [7] for a 3 mm sample containing ~800 ppm of oxygen. We are unable to identify a distinct T_g and hence width of the supercooled regime from the wider portion of the wedge due to the high fraction of crystalline phases present in these regions. The XRD patterns indicate the presence of elemental α-Zr having hexagonal structure, tetragonal Zr_2Cu phase and a dendritic phase in addition to the glassy phase. The proportion of these phases varies along the length of the wedge as shown in Fig. 2.

Figure 3 shows the XRD patterns corresponding to $Zr_{55}Cu_{30}Al_{10}Ni_5$ alloy produced in the form of 3 mm diameter rods and plates of dimension 2×5 mm^2. The as cast rods show the presence of a distinct glassy phase as is evident from the broad hump in addition to α-Zr, Zr_2Cu and the Zr_2Ni phases. The plate sample, in addition, show distinct presence of an oxide phase (ZrO) and have much larger crystalline fraction. Due to the use of split-type Cu

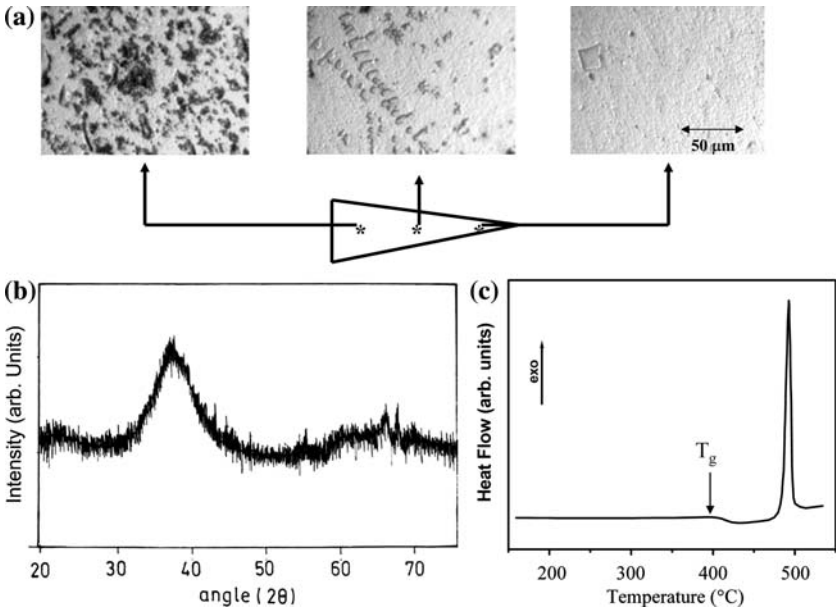

Fig. 1 (**a**) Optical micrographs obtained from various locations (given in the schematic) of the wedge shaped $Zr_{55}Cu_{35}Al_{10}Ni_5$ alloy. (**b**) XRD and (**c**) DSC scans of the material taken from the tip portion of the sample

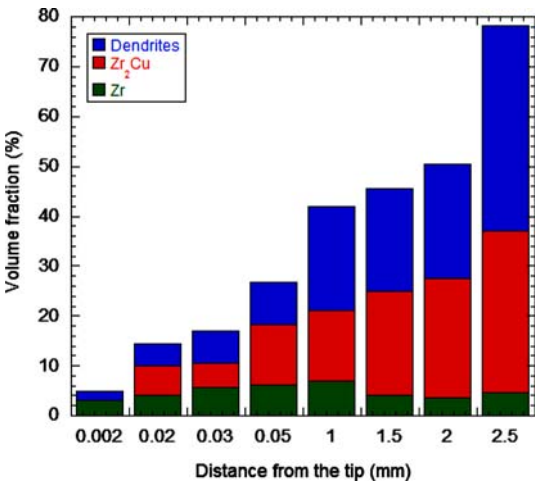

Fig. 2 Variation of the crystalline phases volume fraction as a function of distance from the tip of the wedge shaped $Zr_{55}Cu_{30}Al_{10}Ni_5$ sample

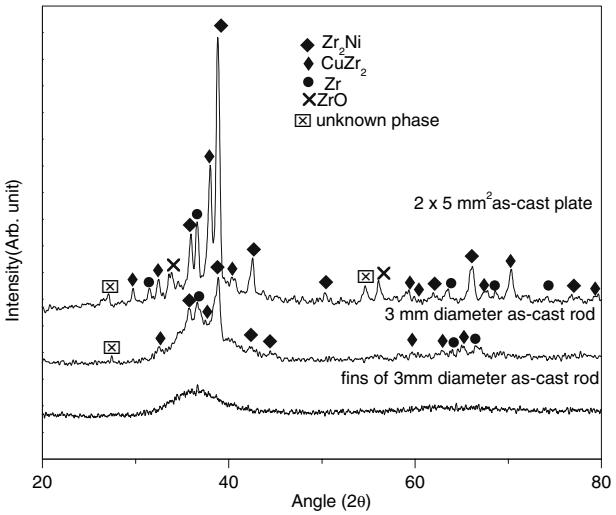

Fig. 3 XRD patterns obtained from different sized castings of $Zr_{55}Cu_{30}Al_{10}Ni_5$ alloy

moulds, fins of thickness ~550 μm had also formed during BMG castings. The XRD patterns corresponding to these fins reveal the presence of broad maxima attesting to its glassy nature. However, a closer examination reveals a small peak of α-Zr.

Figure 4a shows the XRD scans of injection cast alloys with the nominal composition of $Zr_{60}Cu_{20}Al_{10}Ni_{10}$ in the form of 3 and 5 mm diameter rods and 2×3 mm^2 plates. As is evident from the plot, extensive crystallization took place for the plate and 5 mm diameter castings, while the XRD plot for the 3 mm rod exhibits partial presence of a glassy phase. The relatively broader crystalline peaks of the 3 mm samples suggest finer crystalline precipitates. Analysis of the diffraction patterns indicates the precipitation of tetragonal $CuZr_2$ and fcc Zr_2Ni in addition to a small amount of ZrO. There is also evidence of hexagonal α-Zr phase and tetragonal Zr_3Al_2 type phases. Similar casting of $Zr_{65}Cu_{15}Al_{10}Ni_{10}$ alloy however show very high degree of crystallinity irrespective of the casting dimensions (Fig. 4b). The phases identified, though, were almost same as that for the previous alloys, predominantly Zr_2Cu, Zr_2Ni, α-Zr and ZrO, but with an addition of new Zr_2Al_3 type orthorhombic phase. A summary of the DSC results where we have succeeded in detecting the T_g reliably is given in Table 1.

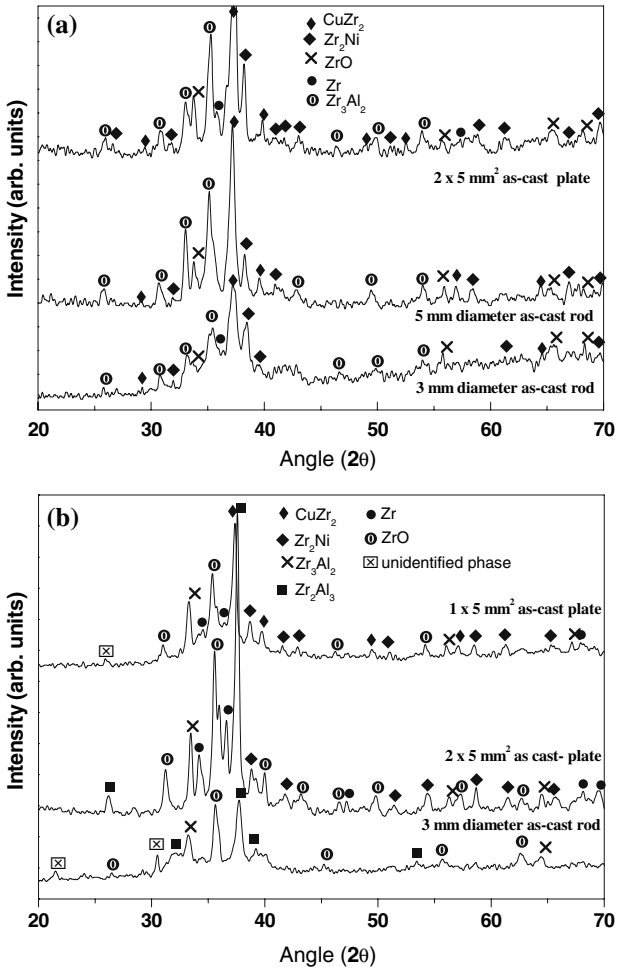

Fig. 4 XRD patterns of alloys with nominal composition (**a**) $Zr_{60}Cu_{20}Al_{10}Ni_{10}$ (**b**) $Zr_{65}Cu_{15}Al_{10}Ni_{10}$ casted in the form of rods and plates

Table 1 A summary of the glass transition (T_g) and crystallization (T_x) temperatures measured by DSC during heating (10 K/s)

Alloy	Casting dimensions	T_g °C	T_x °C	ΔT_x
$Zr_{55}Cu_{30}Al_{10}Ni_5$	3 mm rod	431	460	29
$Zr_{55}Cu_{30}Al_{10}Ni_5$	Wedge, at the tip	408	488	80
$Zr_{60}Cu_{20}Al_{10}Ni_{10}$	Fins	455	470	15

Effect of Y addition

It has been shown that rare earth has potential to scavenge the oxygen and remove the deleterious effect of oxygen [15]. In order to probe whether it is still effective when the oxygen content is high, alloys containing Y and small amount of Ti ($Zr_{53}Cu_{19}Al_{10}Ni_{10}Ti_5Y_3$) with both Zr sponge and high purity Zr crystal as starting materials were prepared. The alloys were suction cast to a 4 mm diameter rod. Figure 5a shows the XRD patterns corresponding to the as-cast $Zr_{53}Cu_{19}Al_{10}Ni_{10}Ti_5Y_3$ alloy prepared with Zr-sponge and high purity Zr respectively. The latter yields a fully glassy structure which is also supported by bright field TEM micrograph in Fig. 5b, which is featureless. Corresponding selected area diffraction (shown in the inset) reveals the typical diffuse halo of an amorphous material. However, the Y addition has significantly improved the glass formation and yielded a partial glassy structure in case of alloy prepared with Zr sponge. The fcc Zr_2Ni is the predominant crystalline phase that was detected, while traces of $CuZr_2$, α-Zr and ZrO were found embedded in the glassy matrix (Fig. 5a). We were unable to obtain any glass at this section thickness without Y addition.

The DSC scan of the alloy prepared with the sponge shows a distinct glass transition as shown in Fig. 5c. It is also interesting to note the single crystallization peak in the DSC, which is characteristic of melts containing lower oxygen content [4]. This further illustrates the success of Y as an oxygen scavenger. Figure 5d shows the scanning electron micrograph corresponding to $Zr_{53}Cu_{19}Al_{10}Ni_{10}Ti_5Y_3$ alloy prepared with Zr sponge showing fine and large dendrites. The EDAX analysis shows that fine dendrites have low content of oxygen while large dendrites have higher oxygen content. From the micrograph (Fig. 5d), it can be noticed that the bigger particles have high oxygen and Y content with low Zr. On the other hand small particles (one of them marked in the figure) contain lower oxygen and major presence of Zr and Cu. However they also contain Al, Ni, Ti and Y as minor alloying elements.

It is important to note here that in addition to the ability to getter oxygen, the addition of 3 at.% Y and 5 at.% Ti represents an increase in the number of components for the multi-component alloy. Therefore, the improved glass formation in the Y and Ti containing BMGs is not only because of the oxygen paralysis but could also be due to—at least partially—the increased number of components in the system and hence decreased propensity for crystallization.

Facets of Zr crystallites

Figure 6a shows a low magnification optical micrograph of the central region of 3 mm injection cast rod of $Zr_{55}Cu_{30}Al_{10}Ni_5$ showing the presence of dispersoids with darker contrast. SEM micrograph of these dispersoids show that they are faceted (Fig. 6b). The EDAX analysis and the X-ray analysis establish them to be α-Zr. The matrix contains colonies of dendrites (Fig. 6c). The fraction of these colonies in the overall microstructure is sensitive to local cooling condition. The dendrites are Zr-rich with Cu as the other main element with average composition of $Zr_{2-x}Cu_{1+x}$ ($x_{max} = 0.3$). However, they also contain small

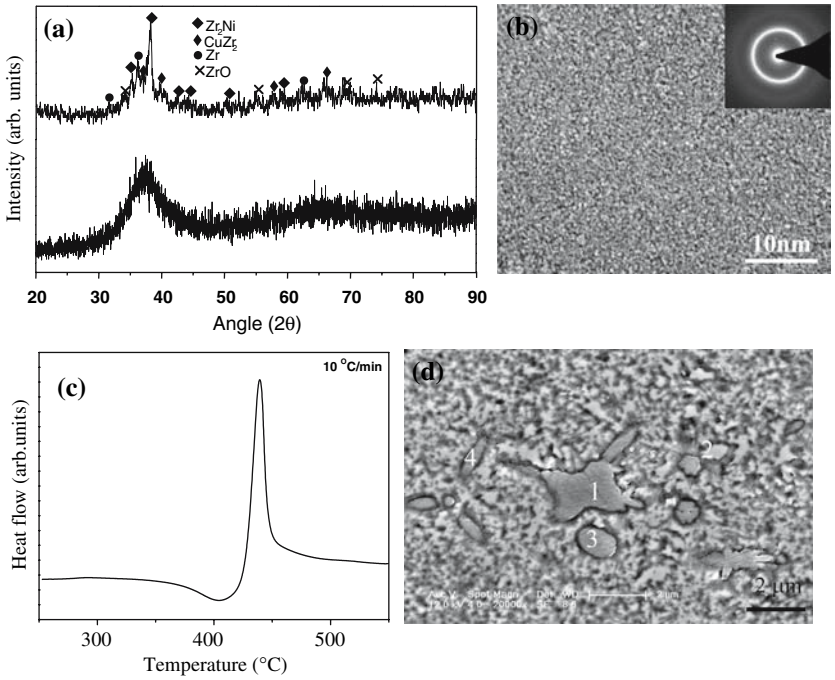

Fig. 5 (**a**) Comparison of the XRD patterns obtained from the $Zr_{53}Cu_{19}Al_{10}Ni_{10}Ti_5Y_3$ alloy prepared with Zr-sponge and high purity Zr. (**b**) and (**c**) are bright field electron micrograph obtained from the latter showing featureless contrast typical to an amorphous material and DSC scan showing a distinct glass transition. Inset in (**b**) shows the corresponding SAD pattern. (**d**) Microstructure of the alloy processed with the Zr-sponge showing fine and large dendrites. The compositions of the different sized particles, marked 1 to 4 have the following compositions, respectively: $Zr_{19.79}Cu_{4.90}Ni_{2.80}Ti_{0.74}AlY_{34.77}O_3$, $Zr_{46.18}Cu_{20.87}Ti_{4.53}Al_{3.91}Ni_{22.17}Y_{0.73}O_{1.77}$, $Zr_{44.37}Cu_{24.89}Ni_{18.96}Al_{4.16}Ti_{4.62}Y_{1.47}O_3$, and $Zr_{22.22}Cu_{13.42}Ti_{3.21}Ni_{9.07}Al_{5.65}Y_{26.76}O_{18.97}$

amount of Al and Ni. Fine dendrites with different contrast can be frequently observed at the core of these dendrite colonies (pointed by arrows in Fig. 6b and c). This is consistent with observations of Gebert et al. [3]. Figure 6d shows the microstructure of the fins. It contains predominantly glassy phase. However, even here one can detect both the α-Zr and Zr_2Cu type of phases. On increasing Zr content additional large dendrites were observed (Fig. 6e). These dendrites are prevalent in high oxygen containing alloys and identified as the orthorhombic Zr_2Al_3 phase from the EDAX results. The peaks of this phase could be observed in the X-ray results obtained from the high Zr alloys. The predominant fcc Zr_2Ni phase is conspicuous by its absence from the SEM micrographs. A possible explanation could be their occurrence as small crystallites of only a few nanometers diameter [3] and hence are beyond the instrumental resolution of the SEM used for this study. The small size of these crystallites is attributed to a high nucleation rate combined with a limited growth rate [16].

Mechanical properties and gradient microstructures

The average hardness of all the Zr–Cu–Ni–Al samples used in this investigation is shown in the Fig. 7. Broadly, the hardness increases with Zr content and with the casting section thickness indicating crystalline products have higher hardness compared to the amorphous phase. This observation is similar to Inoue et al. [17] where they have reported a 37% increase in hardness due to nanocrystalline dispersoids in an amorphous Zr–Al–Ni–Cu–Ag alloy. Basu et al. [18] have also reported that the hardness increases linearly with increasing crystallinity. They have also mentioned the abrupt increase in the elastic modulus when the crystalline volume fraction is about 40 vol.% with an only minor variation on either side of this range. It is also possible that the increase in hardness is also due to an increase in the solute content of the amorphous matrix [19–22].

Since the development of the microstructure in high oxygen content alloys is sensitive to cooling rate, a gradient microstructure is always observed not only in the wedge casting but also in rod and plate. One can utilize this to design gradient samples where the surface is predominantly glassy while the core is crystalline. Figure 8a and b shows the microstructure of a 2 mm section thickness plate casting of a $Zr_{65}Cu_{15}Al_{10}Ni_{10}$ alloy. The surface region is nearly fully amorphous while core is completely crystalline. The fraction of different phases from surface to the center has been estimated and is shown in the histogram (see inset). Figure 8c shows the hardness and the modulus gradation in it. Since crystalline intermetallic phases are

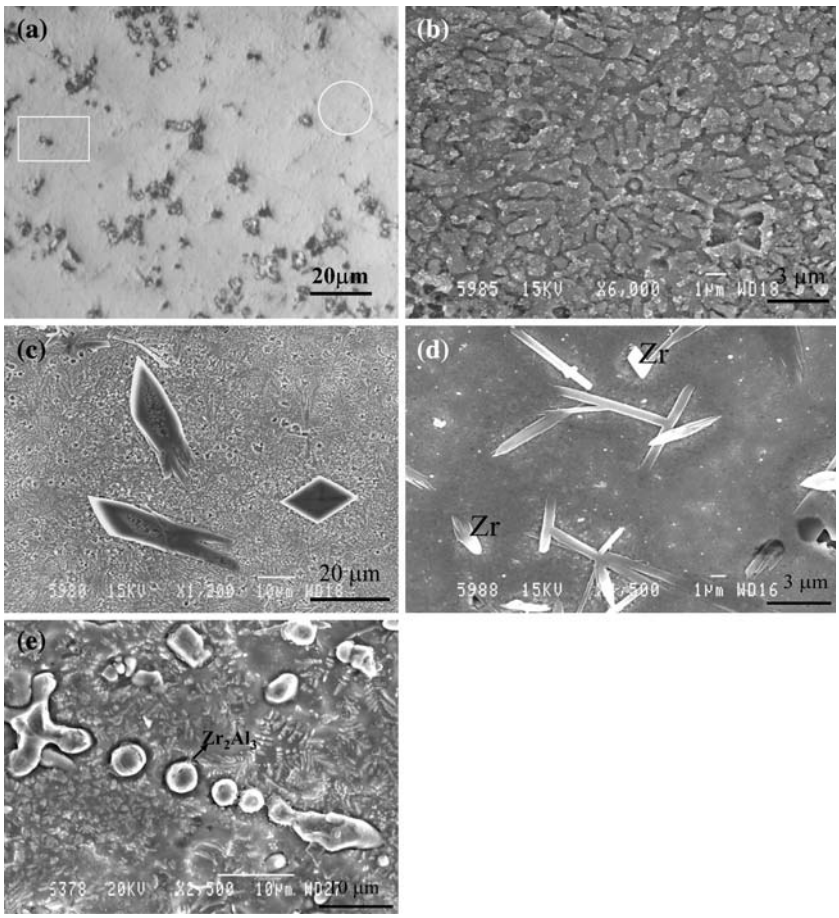

Fig. 6 (**a**) An optical micrograph obtained from the central region of 3 mm injection cast rod of $Zr_{55}Cu_{30}Al_{10}Ni_5$. Magnified SEM images of areas marked by (**b**) rectangle and (**c**) circle. (**d**) and (**e**) are microstructures obtained from the fin portion

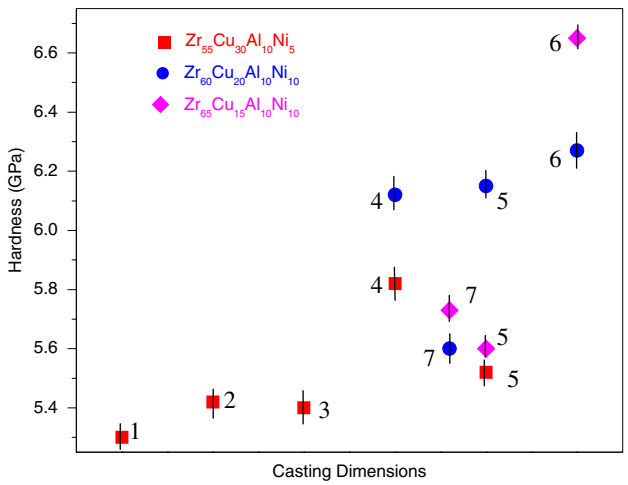

Fig. 7 Hardness data of three different alloys with different casting dimensions. The numbers 1 to 7 refer to the following. (1) as-cast, (2) fin of 3 mm diameter sample, (3) tip portion of the wedge sample, (4) 3 mm diameter rod, (5) 2 × 5 mm^2 plate, (6) 5 mm diameter rods and (7) 1 × 5 mm^2 plate

harder and stiffer, the microstructural gradient leads to a gradient in the mechanical properties. Interestingly, while the elastic modulus appears to vary linearly, the hardness shows a peak at a distance that is ~1 mm away from the center of the plate. Besides the phase fraction, the varying composition due to the partitioning during the solidification process is possibly the reason for this [19].

Discussion

The experimental results presented in the preceding section suggest that the microstructure evolution in Zr–Cu–Al–Ni BMG prepared with commercial sponge and having oxygen contain in excess of 8,000 ppm is different from the BMGs containing less amount of oxygen. Oxygen free BMG of Zr–Cu–Al–Ni decomposes to yield tetragonal $CuZr_2$ and hexagonal $NiAl_2Zr_6$ phases [2, 23]. With addition of oxygen, a metastable cubic phase (Fd3m) of $NiZr_2$ nucleates in the glass homogenously [24, 25]. These fine particles in turn act as the nucleation sites for the heterogeneous nucleation of $CuZr_2$ [3]. This latter phase generally grows as fine dendrites. In melt spun high oxygen containing alloy (>0.6 at.% O), the metastable $NiZr_2$ forms and transforms directly to equilibrium $NiAl_2Zr_6$ phase [3]. Liu et al. [6] have shown the observed metastable cubic $NiZr_2$ phase is most probably Zr_4Ni_2O phase, which forms

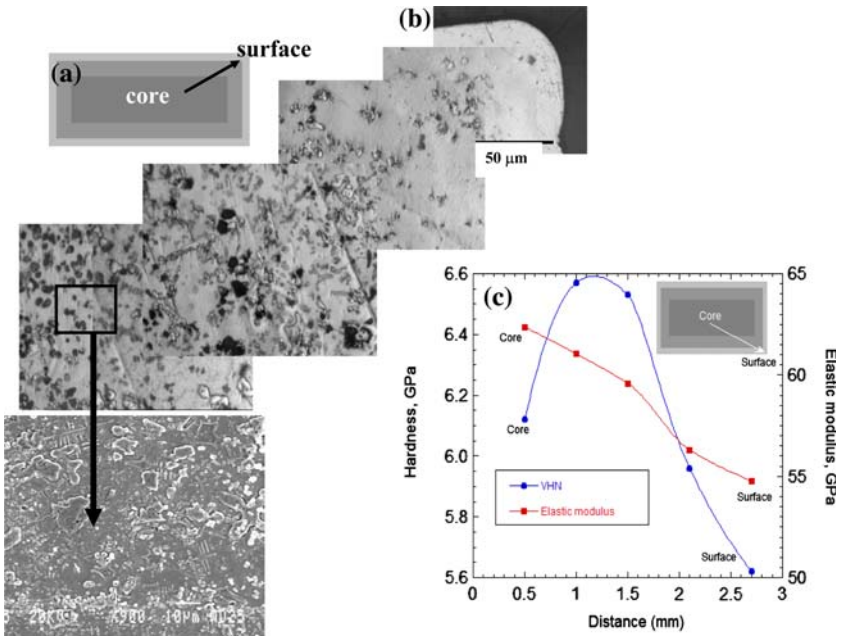

Fig. 8 (**a**) Schematic and (**b**) a collage of optical micrographs of 2×5 mm^2 $Zr_{65}Cu_{15}Al_{10}Ni_{10}$ alloy plate showing a transition from a highly crystalline core to an almost amorphous surface. (**c**) Variation in hardness and elastic modulus with the distance from the core

in the presence of excess oxygen. With increase in oxygen concentration (>8000 ppm) additional phases namely ZrO, Zr_2Al_3 and Zr_3Al_2 appear that are not seen for lower oxygen impurities. The most striking result of a high oxygen content alloy, however, is the formation of α-Zr that forms faceted crystals in all the three alloys. This phase is also not observed at low oxygen content alloy. This suggests that oxygen addition shifts the alloy towards the Zr rich end in the multi component phase field [26].

Conclusions

Higher oxygen concentrations in the melt, obtained from Zr sponge, leads to the formation of phases, which cannot be obtained otherwise by starting off with high purity elements. Oxygen plays a controlling role in developing the microstructure and determining GFA, hence, our results show that dissolved oxygen has to be regarded as an alloying element rather than an impurity. The gradient structure so obtained due to presence of oxygen and varying cooling rates can produce a gradient in mechanical properties.

Acknowledgment Financial support for this work was provided by a grant to IISc by the Defence Research and Development Organization (DRDO), Government of India.

References

1. Lin XH, Johnson WL, Rhim WK (1997) Mater Trans JIM 38:473
2. Eckert J, Mattern N, Zinkevitch M, Seidel M (1998) Mater Trans JIM 39:623
3. Gebert A, Eckert J, Schultz L (1998) Acta Mater 46:5475
4. Murty BS, Ping DH, Hono K, Inoue A (2000) Acta Mater 48:3985
5. Zhang Y, Zhao DQ, Wang RJ, Pan MX, Wang WH (2000) Mater Trans JIM 41:1410
6. Liu CT, Chisholm MF, Miller MK (2002) Intermetallics 10:1105
7. Conner RD, Maire RE, Johnson WL (2006) Mater Sci Engg A 419:148
8. Ping DH, Hono K, Inoue A (1999) In: Johnson WL, Inoue A, Liu CT (eds) Bulk metallic glasses, vol. 554, MRS, Warren dale, PA, p 3
9. Kuebler A, Eckert J, Gebert A, Schultz L (1998) J Appl Phys 83:3438
10. Koester U, Meinhardt J, Ross S, Ruedigger A (1996) Mater Sci Forum 225–227:311
11. Inoue A, Shinohara Y, Yokoyama Y, Masumoto T (1995) Mater Trans JIM 36:1276
12. Frankwicz PS, Ram S, Fecht HJ (1996) Mater Lett 28:77
13. Inoue A, Zhang T, Nishiyama N, Ohba K, Masumoto T (1993) Mater Trans JIM 34:1234
14. Zhang T, Inoue A, Masumoto T (1991) Mater Trans JIM 32:1005
15. Zhang Y, Pan MX, Zhao DeQ, Wang RJ, Wang WH (2000) Mater Trans JIM 41:1410
16. Altounian Z, Guo-hua T, Strom-Olsen JO (1983) J Appl Phys 54:3111
17. Inoue A, Zhang T, Kim YH (1997) Mater Trans JIM 38:749
18. Basu J, Nagendra N, Li Y, Ramamurty U (2003) Phil Mag 83:1747
19. Greer AL (2001) Mater Sci Engng A304–A306:68
20. Nagendra N, Ramamurty U, Goh TT, Li Y (2000) Acta Mater 48:2603
21. Jana S, Ramamurty U, Chattopadhyay K, Kawamura Y (2004) Mater Sci Eng A 375–377:1191
22. Jana S, Bhowmik R, Kawamura Y, Chattopadhyay K, Ramamurty U (2004) Intermetallics 12:1097
23. Koester U, Meinhardt J, Roos S, Busch R (1997) Mater Sci Engg A226–228:995
24. Koester U, Meinhardt J (1994) Mater Sci Engg A 178:271
25. Altounian Z, Shank RJ, Strom-Olsen JO (1985) J Appl Phys 58:1192
26. Mitra S (2000) M.E. Thesis, Indian Institute of Science, Bangalore